# Dual Responsive Photonic Liquid for Independent Modulation of Color Brightness and Hue

| | |
|---|---|
| Journal: | *Materials Horizons* |
| Manuscript ID | MH-COM-04-2021-000556.R1 |
| Article Type: | Communication |
| Date Submitted by the Author: | 02-May-2021 |
| Complete List of Authors: | Liu, Yun; Wuhan University of Technology, State Key Laboratory of Advanced Technology for Materials Synthesis and Processing; University of California Riverside, Department of Chemistry<br>Fan, Qingsong; University of California Riverside, Chemistry<br>Zhu, Guanghao; Wuhan University of Technology<br>Shi, Gongpu; Wuhan University of Technology<br>Ma, Huiru; Wuhan University of Technology,<br>Li, Wei; Wuhan University of Technology<br>Wu, Tianlong; Wuhan University of Technology<br>Chen, Jitao; Wuhan University of Technology<br>Yin, Yadong; University of California Riverside, Department of Chemistry<br>Guan, Jianguo; Wuhan University of Technology, |
| | |

COMMUNICATION

# Dual Responsive Photonic Liquid for Independent Modulation of Color Brightness and Hue†

Received 00th January 20xx,
Accepted 00th January 20xx

DOI: 10.1039/x0xx00000x

Yun Liu,[a, c] Qingsong Fan,[c] Guanghao Zhu,[b] Gongpu Shi,[a] Huiru Ma,*[b] Wei Li,[a] Tianlong Wu,[a] Jitao Chen,[a] Yadong Yin*[c] and Jianguo Guan*[a]

**Responsive chromic materials are highly desirable in the fields of displays, anti-counterfeitings, and camouflages but their advanced applications usually limit by the unrealized delicate and independent tunability in the three intrinsic attributes of color. This work achieves the separate, continuous, and reversible modulation of structural color brightness and hue by an aqueous suspension of dual-responsive $Fe_3O_4$@polyvinylpyrrolidone (PVP)@poly(N-isopropyl acrylamide) (PNIPAM) flexible photonic nanochains. The underlying modulation mechanism of color brightness has been experimentally and numerically deciphered by analyzing their morphological responses to stimuli. When an increasing magnetic field is applied, the random worm-like flexible photonic nanochains gradually orientate along the field direction due to the dominant magnetic dipole interaction over the thermal motion, lengthening the orientation segment length up to the whole nanochains. Consequently, the suspension displays increased color brightness (characterized by diffraction intensity). Meanwhile, its color hue (characterized by diffraction frequency) can be controlled by temperature due to the volume changes of the interparticle PNIPAM. The achieved diverse color modulation steps forward to the next-generation responsive chromic materials and enriches the basic understanding of color tuning mechanisms. With versatile and facile color tunability and shape patterning, the developed responsive chromic liquid promises attractive potentials in full-color displays and adaptive camouflages.**

**New concepts**

The developed responsive chromic materials mainly perform the on-off switch or overall changes in color when stimulated by single or multiple stimuli. Limited by the current color modulation methods, the independent delicate modulation of the three intrinsic attributes of color still remains a challenge. We demonstrate a structural color brightness modulation principle that relies on the dynamic controllability of the periodic range of photonic crystalline structures while remaining their lattice constant unchanged to achieve tunable structural colors with changeable brightness but maintained hue in an aqueous suspension of $Fe_3O_4$@polyvinylpyrrolidone (PVP)@poly (N-isopropyl acrylamide) (PNIPAM) flexible photonic nanochains by changing external magnetic field ($H$). The flexible photonic nanochains with random worm-like conformations exhibit gradually increased periodic ranges along the field direction with increasing field strength due to the dominant magnetic dipole interaction over the thermal motion. Macroscopically, the suspension displays a continuous and rapid response of color brightness to the strength of $H$. Furthermore, the color hue can be adaptively tuned by changing temperature when needed. The achievement of versatile and respective tunability of color brightness and hue by modulating different external stimuli opens an exciting avenue to develop advanced responsive chromic materials.

## Introduction

Color plays an essential role in carrying and covering visual information.[1–3] In nature, some living creatures, such as chameleons, turtle beetles, seahorses, and certain fishes, could utilize their body color changes for information communication, temperature regulation, warning or camouflage, boosting their adaptability to the surrounding environment and survival ability from predators.[4–6] Inspired by these phenomena, a large quantity of responsive chromic materials that change the color in response to external fields, such as light, electric field, magnetic field, temperature, pressure, and chemical agents, have been developed for the growing demands in self-adaptive camouflages, intelligent textiles, sensing, smart displays, energy-saving building materials and fascinating decorations in

---

[a] *State Key Laboratory of Advanced Technology for Materials Synthesis and Processing, International School of Materials Science and Engineering, Wuhan University of Technology, Wuhan 430070, China. *E-mail: guanjg@whut.edu.cn*
[b] *Department of Chemistry, School of Chemistry, Chemical Engineering and Life Science, Wuhan University of Technology, Wuhan 430070, China. *E-mail: mahr@whut.edu.cn.*
[c] *Department of Chemistry, University of California, Riverside, CA 92521, USA. *E-mail: yadong.yin@ucr.edu.*

† Electronic Supplementary Information (ESI) available: Experimental procedures and additional data. See DOI: 10.1039/x0xx00000x

the past decades.[7–20] However, most of them can only carry out the general control of color, especially in the on-off switch or broad frequency ranges.[7–9,15] To meet the critical requirement for their applications in full-color displays, high-security anti-counterfeiting and environmentally adaptive camouflages, developing next-generation responsive chromic materials, which can adaptively modulate the color hue, saturation, and brightness (HSB) in a respective, continuous, and reversible manner by two or multiple independent external stimuli, is indispensable.[4, 21] So far, such responsive chromic materials are not available due to the limitations of the existing color modulation mechanisms or the basic materials. Herein, we report a versatile color-changing aqueous liquid that can independently, continuously, and reversibly tune the color brightness and hue by modulating external magnetic field (*H*) and surrounding temperature (*T*) based on the dual responsive individual photonic nanochains (PNCs) of thermosensitive polymer encapsulating superparamagnetic colloidal nanocrystal clusters (CNCs).

While colors generally stem from chemical colorants, brilliant structural colors can be generated through light-matter interactions such as diffraction, scattering, and interference.[22–24] They are environmental-friendly, energy-saving, and anti-photobleaching, showing increasing importance for future color materials.[25, 26] As typical materials exhibiting structural colors, photonic crystals (PCs) are periodically arranged dielectric materials. The photonic band gaps are in the range of visible spectra when the lattice constants are comparable to the wavelength of visible light.[27] In this case, their diffraction wavelength, diffraction intensity, and peak width at half height correspond to the hue, brightness, and saturation, respectively. When stimuli-responsive materials are used as building blocks or incorporated into the PCs as the surrounding matrix, the band gaps may be tuned by changing the lattice constant, refractive index, or orientation state, endowing them with dynamic tunability of structural colors in response to external stimuli, such as pH, *T*, humidity, electric field and *H*.[28–34] Among them, magnetically responsive PCs have advantages of simple assembly process, reversible and rapid response to *H*, and bright structural colors.[31,35–37] They are based on establishing a balance between magnetic attraction and electrostatic or steric repulsion, thus displaying tunable color hues covering the entire visible spectra.[38–40] The one-dimensional periodically arrayed structures of superparamagnetic CNCs could be fixed by inorganic materials or polymers, producing various forms of one-dimensional magnetic PCs including films,[41] balls,[30,42–44] fibers,[4,5] and individual PNCs.[46–50] They can display either constant structural colors or tunable colors with overall changes in HSB when stimulated by a single external field.

In this paper, the independent, continuous, and reversible modulation of structural colors in brightness and hue has been demonstrated by an aqueous suspension of magnetically and thermally responsive $Fe_3O_4$@polyvinylpyrrolidone (PVP)@poly(N-isopropyl acrylamide) (PNIPAM) flexible PNCs. As indicated by both the experiment and numerical simulation results, the continuous and reversible tunability of color brightness at constant color hue benefits from the flexibility of encapsulated PNIPAM and the large chain length, which guarantee the gradual domination of magnetic interaction over thermal motion with increasing *H* and enable the orientation and stretch of the chains along the field direction. Consequently, the flexible PNCs exhibit better periodic structures along the field direction under stronger *H*, leading to enhanced color brightness. Meanwhile, the versatile controllability of color hue could be achieved due to the thermally responsive property of the linking PNIPAM, which adjusts the interparticle distance by volume changes with *T*. The realization of diverse tunability of structural color in brightness and hue is expected to help develop next-generation chromic materials and enrich the basic understanding of structural color modulation mechanisms. The obtained dual responsive liquid shows great potential for smart structural color materials.

## Results and Discussion

A dual-responsive aqueous dispersion of $Fe_3O_4$@polyvinylpyrrolidone (PVP)@poly(N-isopropyl acrylamide) (PNIPAM) flexible photonic nanochains (PNCs) has been used to investigate the independent, continuous, and reversible modulation of color brightness and hue. The monodisperse $Fe_3O_4$@PVP colloid nanocrystal clusters (CNCs) with an average diameter of 140 nm (Fig. S1, ESI†) were used as building blocks of the $Fe_3O_4$@PVP@PNIPAM flexible PNCs, which were fabricated by a hydrogen bond-guided template polymerization method.[49] As shown in Fig. 1a, the formation procedure of the $Fe_3O_4$@PVP@PNIPAM flexible PNCs includes the self-assembly of $Fe_3O_4$@PVP CNCs induced by external *H* and the following *in situ* polymerization of NIPAM initiated by UV light. In the reaction system, PAA functions as a bridge between PVP and NIPAM by forming hydrogen bonds.[49] The formation procedure could be illustrated as follows: First, PAA forms hydrogen bonds with PVP and NIPAM, leading to a much higher NIPAM concentration within the PVP brush shells of $Fe_3O_4$@PVP CNCs than that outside in the solution. Then, the CNCs with NIPAM within the PVP shells aligned along *H* with a nearly equal interparticle distance when an external *H* was applied. Finally, the polymerization of NIPAM on the $Fe_3O_4$ particle surface and the interparticle regions was initiated by UV light, resulting in individual one-dimensional periodical nanochains linked by polymers. The addition and amount of PAA significantly influence the formation of the flexible PNCs because it determines the amount of NIPAM absorbed on the surface of the $Fe_3O_4$@PVP CNCs. The product obtained without the addition of PAA (Fig. S2a, ESI†) exhibits monodisperse sphere morphology with rough surface, which shows no obvious difference compared to the initial $Fe_3O_4$@PVP CNCs (Fig. S1, ESI†), indicating the poor interaction between PVP and NIPAM. When the PAA concentration is 0.31 $mg \cdot mL^{-1}$, nanochains with perfect chain structure still could not be obtained due to the insufficient surface coating of PNIPAM. (Fig. S2b, ESI†) When the PAA concentration is further increased to 1.67 $mg \cdot mL^{-1}$, the flexible PNCs could be obtained but they tend to form bundle chains with thick polymer shells. (Fig. S2c, ESI†) The slightly decreased interparticle distance within the nanochains

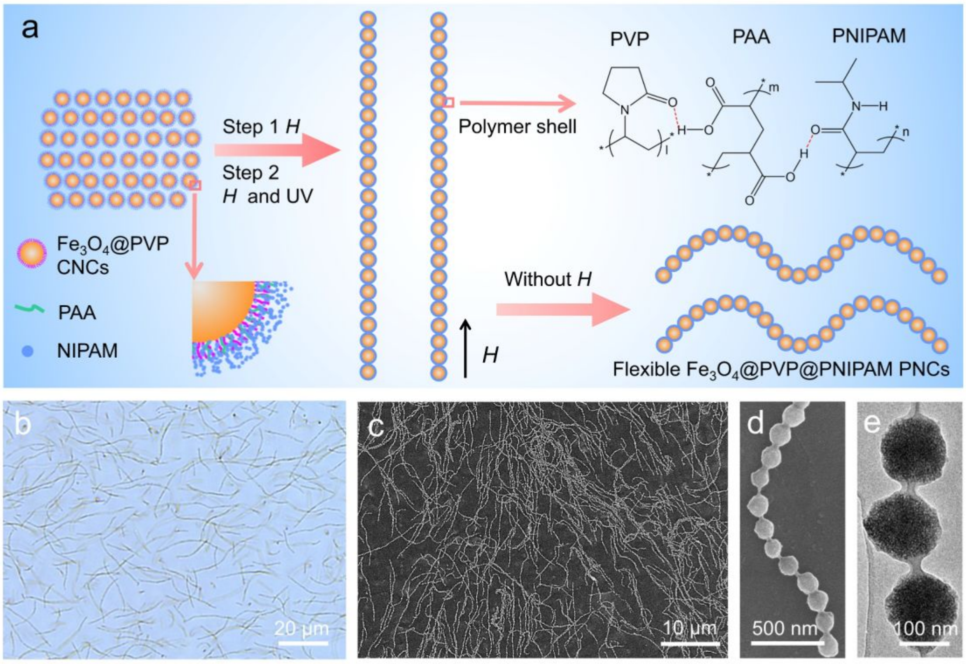

**Fig. 1** The preparation and characterization of the typical $Fe_3O_4$@PVP@PNIPAM flexible PNCs. (a) Schematic illustration showing the formation process of the $Fe_3O_4$@PVP@PNIPAM flexible PNCs; (b) Bright-field optical microscopy image, (c, d) SEM images, (e) TEM image.

obtained at high PAA concentration was caused by the compression of the PVP brush shells due to their strong interaction with PAA.

The bright-field optical microscopy image and scanning electron microscope (SEM) images (Fig. 1b and c and Fig. S3a, ESI†) clearly show that the products of individual nanochains exhibit a randomly natural bending state with an average end-to-end distance (*D*) of about 13 μm. When an external magnetic field (*H*) is applied, the nanochains could align along the field direction with the average chain length (*L*) up to about 15 μm, larger than *D* (Fig. S3b, c, ESI†). This confirms the polymer-analogous flexibility of the nanochains. The magnified SEM image (Fig. 1d), TEM image (Fig. 1e), and the FT-IR spectrum (Fig. S4a, ESI†) reveal that the nanochains are pearl necklace-like structures, in which the particle cores are coated and separated by a PNIPAM layer. The exact mass percentage of polymers was calculated as 34.37% based on the TG-DSC data (Fig. S4b, ESI†). Furthermore, the superparamagnetic property of the obtained $Fe_3O_4$@PVP@PNIPAM flexible PNCs, which endows their reversible magnetically responsive property, is confirmed by the magnetic hysteresis loop (Fig. S4c, ESI†), showing negligible remanent magnetization ($M_r$) and coercivity ($H_c$) with a mass saturation magnetization ($M_s$) of 33.09 $emu{\cdot}g^{-1}$.

The aqueous suspension of the obtained $Fe_3O_4$@PVP@PNIPAM flexible PNCs exhibits independent, continuous, and reversible tunability of diffraction intensity and diffraction wavelength under different *H* and temperature (*T*). As seen from Fig. 2a, the aqueous suspension of the typical $Fe_3O_4$@PVP@PNIPAM flexible PNCs at 6 °C exhibited yellow color but enhanced brightness with increasing *H*. At *H* = 10 Gs, only a dark yellow color appeared. When *H* was increased to 50 Gs, a homogeneous color could be observed. The color became much brighter when *H* was further enhanced to 100 and 400 Gs. The 2D contour map of the reflection spectra (Fig. 2b) confirms that the flexible PNCs under different *H* show the same diffraction peak at around 600 nm, but the reflectance (*R*) increases with the increase of *H*, consistent with the dark-field optical microscopy observation. This completely distinguishes it from that of the rigid straight magnetic counterparts, of which the structural color brightness is almost independent of the strength of *H*. According to Bragg's law:

$$\lambda = 2nd\sin\theta \qquad (1)$$

where $\lambda$ is the diffraction wavelength, *n* is the relative refractive index, *d* is the lattice spacing, and $\theta$ is the angle between the incident light and the line perpendicular to the axes of the PNCs,[51] the maintained diffraction peaks are beneficial from the unchanged interparticle distance under a constant temperature. The slight blue shift of diffraction peak at 10 Gs may be explained by the fact that the external *H* of 10 Gs is too low to get well-ordered oriented segments within the flexible chains so that the value of $\theta$ deviates from 90°. When *T* was set to 30 °C, the flexible PNCs also show the same changing trend of color brightness with *H,* but the diffraction peak blue-shifted to green (560 nm) compared with the case at 6 °C (Fig. 2c and d). Movie S1 (ESI†) shows the dynamic changes of color brightness with *H*. It was observed that the color brightness rapidly enhanced as *H* increased from 0 to 400 Gs and then synchronously faded out as *H* decreased from 400 to 0 Gs, indicating that the tuning of color brightness was a continuous, reversible, and rapid process. When *T* was further increased to 37 °C, the flexible PNCs still demonstrate increased brightness with the enhancement of *H* but with the diffraction color further shifted to blue (Fig. S5, ESI†). This suggests a universal phenomenon for the typical flexible PNCs to exhibit magnetic field strength-dependent diffraction intensity.

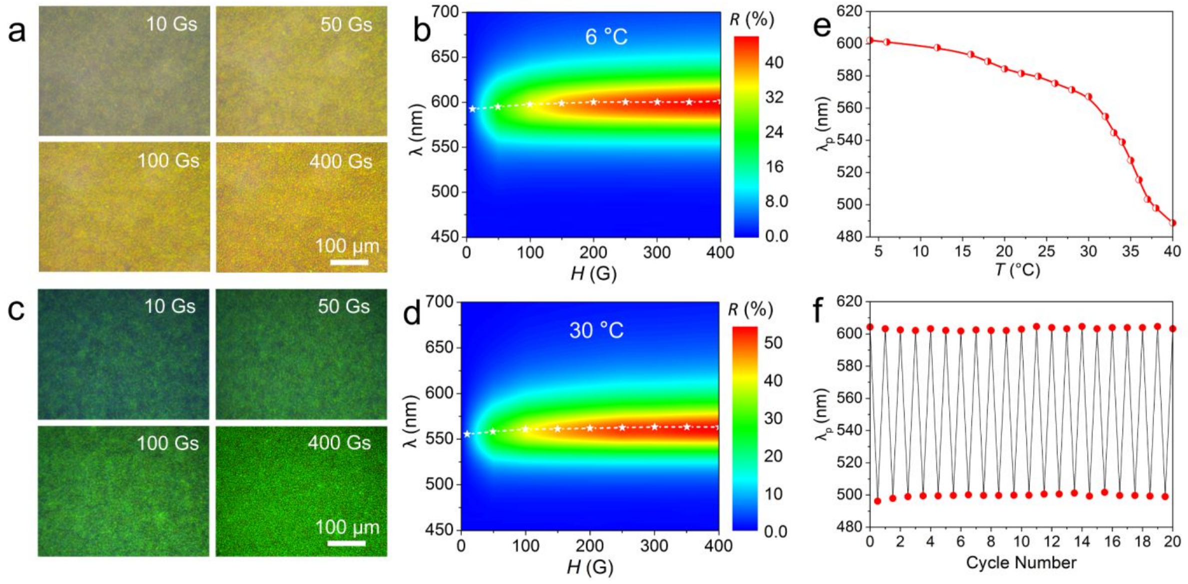

**Fig. 2** The dual responsive optical properties of the typical $Fe_3O_4$@PVP@PNIPAM flexible PNCs. (a, c) Dark-field optical microscopy images and (b, d) 2D contour maps of reflection spectra obtained under different *H* and *T*. (a, b) 6 °C; (c, d) 30 °C. (e) Diffraction wavelength as function of *T*. (f) Cycling performance showing the variation of diffraction peaks between 4 and 38 °C for 20 times. The magnetic field direction in (a, c) is parallel to the observation direction.

The dynamic changes of color hue with *T* were shown in Movie S2 and Movie S3 (ESI†). When the sample was stimulated by a drop of ice water (4 °C), the diffraction color changed from green to yellow (Movie S2, ESI†). When it was stimulated by a drop of 40 °C warm water, the diffraction color rapidly changed from green to blue and then recovered to green (Movie S3, ESI†), showing reversible tunability of color hue. The shift of diffraction color was attributed to the thermosensitive property of PNIPAM, which exhibits a reversible transition between the hydrophilic state and hydrophobic state as *T* changes.[52] When stimulated by warm water, the PNIPAM in the interlayer and shell of the nanochains experienced a rapid shrunk by expelling water out, leading to a decrease of the interparticle distance and thus the blue shift of diffraction color. When *T* is recovered to room temperature, PNIPAM returned to a swelling state, leading to increased interparticle distance and the corresponding recovery of structural color. The as-obtained flexible PNCs showed a more rapid color change speed than the corresponding thermochromic films and balls,[44,53] which can be illustrated by their reduced volume change relaxation time[54]:

$$\tau = A^2\pi^{-2}S^{-1} \qquad (2)$$

where *A* is the characteristic length and *S* is the corresponding diffusion coefficient. For the flexible PNCs with a tens-of-nanometer-thick peapod-like PNIPAM shell, *A* could be effectively reduced, ensuring their rapid thermo-responsive property. As shown in Fig. 2e, the diffraction peak ($\lambda_p$) blueshifts from 602 to 489 nm as *T* increases from 4 to 40 °C. The diffraction peak exhibits a rapid decrease at around 32 °C, corresponding to the lower critical solution temperature (LCST) of PNIPAM. Furthermore, the thermo-responsive property is reversible and shows good recycling performance (Fig. 2f). The above results indicate that the obtained aqueous suspension of $Fe_3O_4$@PVP@PNIPAM flexible PNCs achieves the modulation of structural color in both brightness and hue in an independent, continuous, and reversible manner, which essentially diverse and enrich the tunability of structural color. The advantages of versatile shape patterning and adaptive color tuning of the obtained structural color liquid endow their great potential applications in full-color displays, sensors, and camouflages.

To understand the magnetic field strength-dependent optical properties of the flexible PNCs, we recorded *R* versus magnetic field induction time (*t*) under different *H*. As shown in Fig. 3a, with the extension of *t*, *R* quickly increases before reaching a constant maximum value ($R_{max}$). Increasing *H* enhances $R_{max}$ but reduces the shortest time needed for the corresponding $R_{max}$ ($t_{min}$). $t_{min}$ is almost on the second scale if *H* is stronger than 10 Gs, and typically less than 1 s at *H* stronger than 100 Gs. This confirms the swift response of the PNCs to *H*. As depicted in Fig. 3b, the correlation of $t_{min}$ and $R_{max}$ with *H* can be well fitted by the Boltzmann function model, implying that the incorporation of magnetic energy balances the thermal motion of the flexible PNCs, leading to the improvement of $R_{max}$. The diffraction intensity tunability of the flexible PNCs with *H* may benefit from their polymer-like flexibility and superparamagnetic property, enabling them to become ordered structures segment by segment with the increasing of *H*.

To intuitively substantiate the above assumption, we used optical microscopy to directly observe the orientation process of the flexible PNCs. As shown in Fig. 3c and Movie S4 (ESI†), when a weak *H* of 50 Gs was applied, the randomly dispersed flexible PNCs partly orientated along the field direction as *t* increased from 0 to 5 s, but they still have bent segments that could not be stretched to a straight state. When *t* was extended to 10 s, the PNCs did not show obvious changes in the conformation except for small fluctuations, indicating that the complete stretch orientation could not be achieved at low *H* by prolonging *t*, in accordance with the optical property results (Fig. 3a). Fig. 3d records the balance conformations of the flexible PNCs under different *H*. Most of the PNCs did not achieve the deflection orientation along *H* under 10 Gs. When

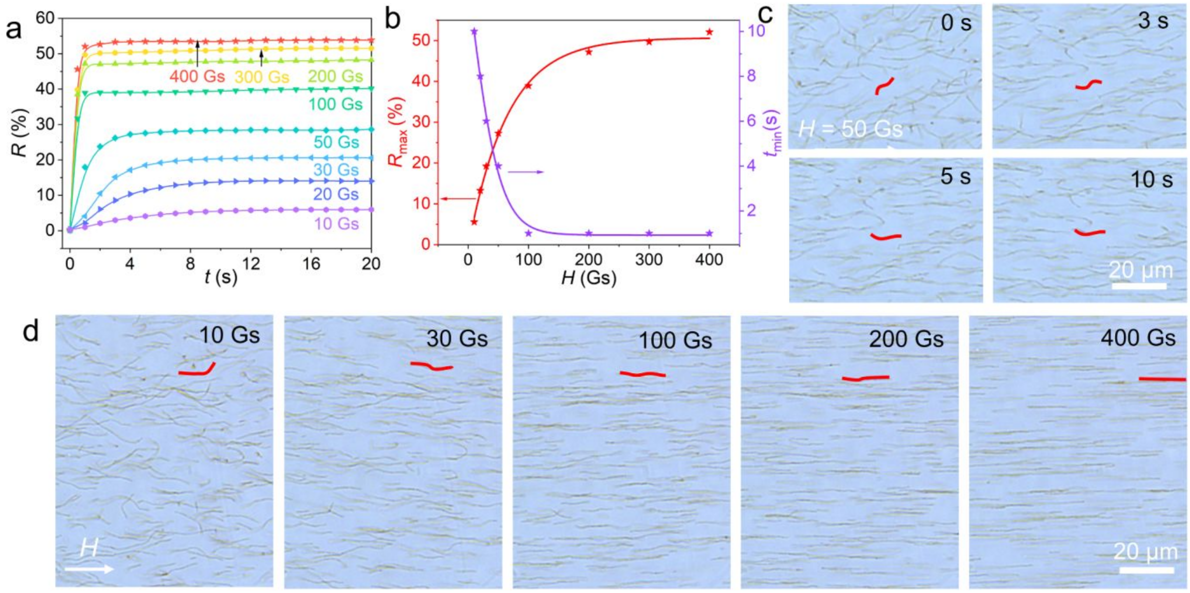

**Fig. 3** The influence of $H$ and $t$ on the reflectance and orientation of the typical $Fe_3O_4$@PVP@PNIPAM flexible PNCs. (a) $R$ as a function of $t$ under different $H$. (b) The influence of $H$ on the corresponding maximum reflectance ($R_{max}$) and the shortest time needed for $R_{max}$ ($t_{min}$). The solid lines are the fitting results of the $R_{max}$ and $t_{min}$ data as a function of $H$ based on the Boltzmann model. (c) Bright-field optical microscopy images obtained under 50 Gs with different $t$. (d) Bright-field optical microscopy images obtained under different $H$ with $t$ = 10 s. Typical nanochains were highlighted in red in (c) and (d) to ease the observation.

$H$ was increased to 20 and 30 Gs, the flexible PNCs started to orient along $H$ but existed in an obvious bending state, indicating that the energy supplied by the weak magnetic field is insufficient to balance the thermal motion of most segments and stretch the bent chains. When $H$ was further enhanced to 100 and 200 Gs, most of the flexible long PNCs performed stretch orientation with a few bent segments. All the PNCs were stretched entirely to a straight state at $H$ = 400 Gs. The small movement towards the field direction under strong $H$ is caused by the magnetic packing force induced by the inhomogeneous magnetic field supplied by a magnet during the observation process. Careful observation indicates that short PNCs are easier to facilitate the complete orientation along $H$ than the long ones, suggesting the stronger $H$ dependence of the optical properties of the long flexible PNCs than the short ones. Movie S5 and Movie S6 (ESI†) show the dynamic orientation process of the flexible PNCs under 400 Gs and varying $H$ from 0 to 400 to 0 Gs, respectively. They confirm the rapid orientation under strong $H$ and a continuous, reversible, and controllable orientation transformation with $H$, resulting in the tunable periodicity and optical properties of the long flexible PNCs with $H$.

Based on the microscopy observation, we assume a schematic illustration for the orientation process of the flexible PNC under $H$ (Fig. 4a). Flexible long PNCs exhibit random worm-like conformations due to the large entropic elasticity endowed by the thermal motion of the flexible PNIPAM gels, similar to the case of flexible polymer chains associated with the rotation of C-C bonds caused by thermal disturbance.[55,56] When an external $H$ is applied, the superparamagnetic $Fe_3O_4$ CNCs in the chain acquire an induced dipole moment:

$$\boldsymbol{m} = \frac{4}{3}\pi r_0^3 \mu_0 \chi \boldsymbol{H} \tag{3}$$

where $\mu_0$ is the vacuum magnetic permeability, $r_0$ and $\chi$ are the particle radius and volume susceptibility, respectively. [36] Thus, both the dipole-dipole interaction force:

$$\boldsymbol{F}_{\rm d} = 3m^2(1-3\cos^2\alpha)\boldsymbol{r}d^{-4} \tag{4}$$

($\alpha$ is the angle between the line connecting the two dipoles and the magnetic field direction, $\boldsymbol{r}$ is the unit vector parallel to the line pointed from two adjacent particles, and $d$ is the center-to-center distance of the two adjacent particles) and the dipole-field packing force:

$$\boldsymbol{F}_{\rm P} = \nabla(\boldsymbol{mH}) \tag{5}$$

are induced to minimize the magnetic potential energy.[31,57] When they surmount the entropic elasticity of a segment of the flexible PNC, the segment stretch orientation occurs along $H$. The orientated length could be gradually extended by further enhancing $H$. Thus, the whole flexible PNCs could orientate along $H$ when $H$-induced $F_d$ and $F_p$ are strong enough to balance the entropic elasticity of the whole flexible PNC, ensuring the long-range ordered structure of the entire PNC.

The relationship between the magnetic field strength and the conformation of the flexible PNCs was qualitatively illustrated by a quasi-3D simulation experiment, which gives the probabilities of different chain conformations based on their total energy. The total energy of each flexible PNC under a certain $H$ was calculated by considering the Weeks–Chandler–Andersen (WCA) interaction, bonded interaction, and magnetic dipole-dipole interaction.[58,59] With the calculated energy of each conformation, their probabilities were evaluated from the partition function. A detailed description of the model (Fig. S6, ESI†) and the conformation probability calculation are shown in the ESI†. It shows that most conformations exhibit similar probabilities without $H$ (Fig. S7, ESI†), consistent with the randomly dispersed bending states of the flexible PNCs. The few blue dots in the center area indicate

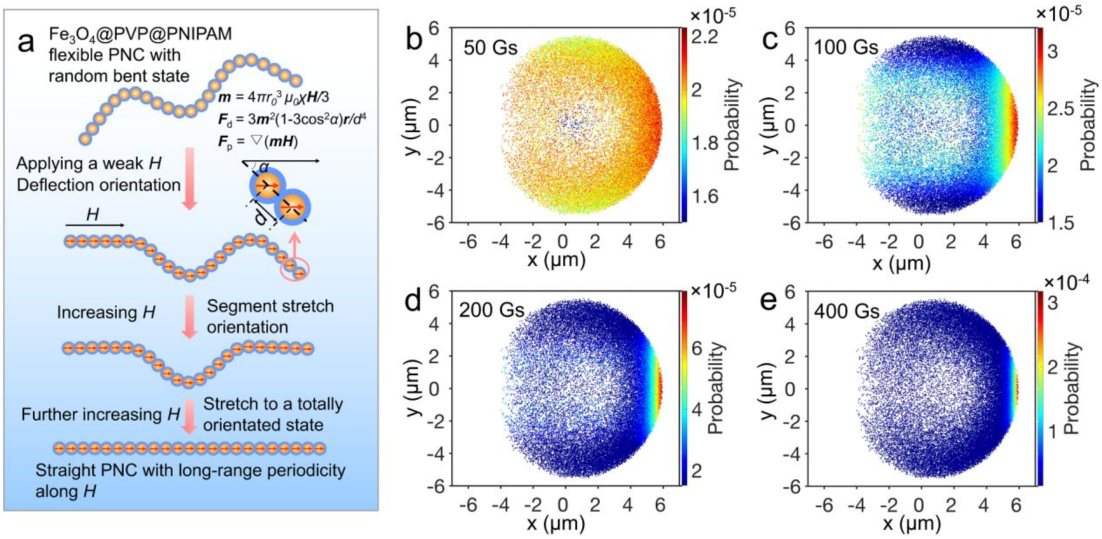

**Fig. 4** (a) Schematic illustration for the orientation process of flexible PNC under *H*. (b-e) The calculated probabilities of different conformations that 50,000 flexible PNCs show under different *H*.

that the probabilities of the corresponding conformations are close to 0 due to the high repulsive WCA potential caused by the overlapping of spheres in those conformations. When a weak magnetic field (50 Gs) is applied along the positive x-direction, the chains with ends at the right side have higher probabilities than those with ends at the top or bottom sides (Fig. 4b). The change of the conformation probabilities with *H* (Fig. 4b–e) reveals that it becomes more obvious for the PNCs to align themselves along the direction of *H* to minimize the total energy of the system. When *H* = 400 Gs, there are much larger probabilities for the PNCs to have ends at the right-most side than at other positions, indicating the most stable conformation of the self-aligned straight state under strong *H*, consistent with the experimental observations and the assumption illustrated in Fig. 4a. This reveals that due to the superparamagnetic property of the CNCs, the flexibility of the PNIPAM shells and linkers, and the characteristic large chain length, the flexible PNCs could exhibit balanced states with aligned segments of different length along *H*, showing unique *H*-dependent diffraction intensity and color brightness.

As observed from the optical images (Fig. 3d), the smaller the chain lengths, the faster the total orientation occurs along *H*. Thus, for the flexible PNCs with different average chain lengths (Fig. S8, ESI†), the short ones show a more rapid increase in the relative reflectance ($R/R_{\max}$) values with the enhancement of *H* than the long ones (Fig. 5a). The higher $R/R_{\max}$ values for short PNCs under weak *H* are attributed to their limited disordered segments and rapid total orientation along *H*, showing the limited tunning ability of diffraction intensity, consistent with the optical observations. In contrast, long flexible PNCs possess much more disordered segments, which can be stretched to an orientated state gradually by increasing *H*, guaranteeing their long-range periodic structure under strong *H*, which is beneficial to obtaining high reflectance and bright brightness. The results further approve that the large chain length is essential for the flexible PNCs for their magnetic field strength-dependent tunability in color brightness.

In addition to the large chain length, the magnetic field strength-dependent diffraction intensity of the $Fe_3O_4$@PVP@PNIPAM PNCs flexible PNCs also benefits from their flexibility originating from the soft property of the linking PNIPAM. The flexible PNCs with different cross-linking degrees were obtained by tuning the molar ratio of BIS and NIPAM ($\delta$) during the preparation procedure (Fig. S9, ESI†). As seen from Fig. S10 (ESI†), the flexible $Fe_3O_4$@PVP@PNIPAM PNCs with $\delta$ = 2%, 5%, and 10% all show a magnetic field tunable diffraction intensity due to the intrinsic soft property of PNIPAM. When *H* = 0–50 Gs, the PNCs with $\delta$ = 10% exhibit bigger $R/R_{\max}$values than those with $\delta$ = 2% and 5%, which only show negligible difference with irregular fluctuations. When *H* = 50–400 Gs, the $R/R_{\max}$values for the PNCs under a certain *H* increase as $\delta$

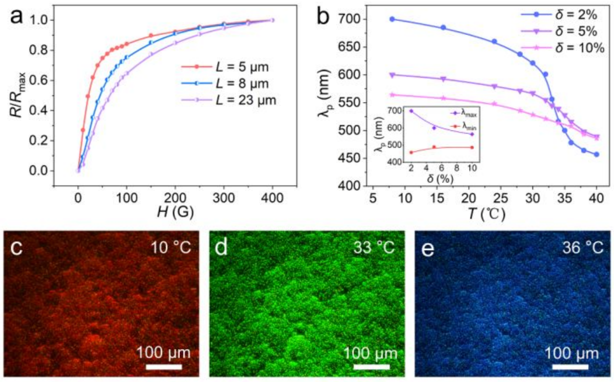

**Fig. 5** The influence of *L* and $\delta$ on the optical properties of the $Fe_3O_4$@PVP@PNIPAM flexible PNCs. (a) Plots showing the magnetic field strength responsive optical properties of the flexible PNCs with different *L*. (b) Plots showing the temperature-responsive optical properties of the flexible PNCs with different $\delta$. The inset in (b) shows the maximum and minimum diffraction wavelengths of the flexible PNCs with different $\delta$. (c–e) Dark-field optical microscopy images of the flexible PNCs with $\delta$ = 2% under different temperature.

increases from 2% to 5% but decrease as $\delta$ further increases from 5% to 10%. The rapid increase of $R/R_{\max}$ values for the PNCs with $\delta$ = 10% at weak $H$ is attributed to their rapid rotation orientation along the field direction, which benefits from their less bending original conformations. With the increase of $H$, the orientation of the flexible PNCs is dominated by the segment stretch orientation along $H$, the PNCs with lower $\delta$ possess more disordered segments, showing a slower increase in $R/R_{\max}$ values. However, flexible PNCs with $\delta$ = 10% exhibit a decreased sensitivity of magnetic field strength due to their reduced flexibility and high magnetic energy needed for the stretch of segments with enhanced mechanical strength. The flexible nanochains with different cross-linking degrees under a certain $H$ slightly differ the $R/R_{\max}$values from an overall perspective. This phenomenon could be reasonably explained by the full consideration that the PNCs obtained with different $\delta$ have different intrinsic soft attribute of PNIPAM, and different lattice distances and polymer content of the PNCs.

While the crosslinking degree of the flexible $Fe_3O_4$@PVP@PNIPAM PNCs does not significantly influence their magnetic field strength-responsive optical property, their temperature-responsive optical property is obviously affected. Fig. 5b shows that the tuning range of diffraction wavelength decreases from 243 to 78 nm as $\delta$ increases from 2% to 10%. The maximum diffraction wavelength ($\lambda_{\max}$) for the flexible PNCs of different $\delta$ decreases with increasing $\delta$. In contrast, the minimum diffraction wavelength ($\lambda_{\min}$) increases first as $\delta$ increases from 2% to 5% and then remains nearly constant as $\delta$ further increases from 5% to 10%. The higher $\lambda_{\max}$ and lower $\lambda_{\min}$ for flexible PNCs with $\delta$ = 2% indicate their larger and smaller interparticle distance at low and high temperatures. This confirms that the low crosslinked flexible PNCs show strong swelling or shrinking ability due to the loose structure of the polymer networks, guaranteeing their good temperature responsiveness. The flexible PNCs with $\delta$ = 2% achieved tunable hues ranging from red to blue (Fig. 5c–e), and their continuous and reversible temperature-responsive color change progress was shown in Movie S7 (ESI†) The results demonstrate that the tunability of the color hue covering the entire visible light spectrum can be achieved by simply adjusting the crosslinking degree of the linking PNIPAM. Furthermore, the $Fe_3O_4$@PVP@PNIPAM flexible PNCs with original diffraction colors ranging from red to blue could be easily obtained by tuning the reaction parameters during the sample fabrication progress (Fig. S11, ESI†), which could be utilized to control the structural parameters of the flexible PNCs and thus their dual-responsive properties. By combining the delicate fabrication and the respective or combination stimuli of magnetic field and temperature, targeted structural colors with independent, continuous, and reversible modulation in brightness and hue can be achieved by the developed aqueous suspension of the $Fe_3O_4$@PVP@PNIPAM flexible PNCs.

## Conclusions

In summary, the independent, continuous, and reversible modulation of structural colors in brightness and hue has been achieved by an aqueous suspension of dual responsive $Fe_3O_4$@PVP@PNIPAM flexible PNCs. Benefited from the superparamagnetic property of $Fe_3O_4$@PVP CNCs, the soft nature of the linking PNIPAM, and the large chain length, the as-obtained flexible PNCs show gradual stretching orientation along the field direction due to the domination of their magnetic potential energy over their entropic elasticity in an enhancing external magnetic field, ensuring the enhancement of diffraction intensity and structural color brightness. The tunability of structural color brightness of the flexible PNCs relies on their large chain-length and flexibility. Meanwhile, the hue of the flexible PNCs can be easily tuned by changing the surrounding temperature due to the temperature-dependent volume shrinking or swelling behavior of PNIPAM. Furthermore, the delicate fabrication of the flexible PNCs with different original colors and the single or combined stimuli of magnetic field and temperature could be utilized to achieve targeted colors with predesigned brightness and hue. The independent, continuous, and reversible tunability of structural colors in brightness and hue of the developed photonic liquid promises the next-generation adaptive chromic materials and enriches the basic understanding of color modulation mechanisms.

## Author contributions

J. G. and H. M. conceived the idea and designed the experiments. H. M., Y. Y. and J. G. supervised the project. Y. L., G. Z., G. S. and J. C. conducted the experiments and analyzed the results. Y. L., Q. F., W. L. and T. W. designed and conducted the simulation calculations. Y. L. and Q. F. wrote the manuscript. H. M., Y. Y. and J. G. revised the manuscript. All authors contributed to the discussion and preparation of the manuscript.

## Conflicts of interest

There are no conflicts to declare.

## Acknowledgments

This work was financially supported by the National Key R&D Program of China (2020YFA0710100), the National Natural Science Foundation of China (51521001), the Natural Science Foundation of Hubei Province (2019CFB572), the Fundamental Research Funds for the Central Universities (WUT: 2017-YB-003), and the China Scholarship Council (CSC). Yin is grateful for the financial support from the US National Science Foundation (DMR-1810485).

## References

1 P. Wu, J. Wang and L. Jiang, *Mater. Horiz.*, 2020, **7**, 338–365.
2 C. Fenzl, T. Hirsch and O. S. Wolfbeis, *Angew. Chem. Int. Ed.*, 2014, **53**, 3318–3335.
3 E. S. A. Goerlitzer, R. N. K. Taylor and N. Vogel, *Adv. Mater.*, 2018, **30**, 1706654.
4 L. Shang, W. Zhang, K. Xu and Y. Zhao, *Mater. Horiz.*, 2019, **6**, 945–958.

5 J. Teyssier, S. V. Saenko, D. van der Marel and M. C. Milinkovitch, *Nat. Commun.*, 2015, **6**, 6368.

6 Y. Zhao, Z. Xie, H. Gu, C. Zhu and Z. Gu, *Chem. Soc. Rev.*, 2012, **41**, 3297–3317.

7 A. Abdollahi, H. Roghani-Mamaqani and B. Razavi, *Prog. Polym. Sci.*, 2019, **98**, 101149.

8 A. Abdollahi, H. Roghani-Mamaqani, B. Razavi and M. Salami-Kalajahi, *ACS Nano*, 2020, **14**, 14417–14492.

9 Y. Wang, Q. Zhao and X. Du., *Mater. Horiz.*, 2020, **7**, 1341–1347.

10 T. H. Park, H. Eoh, Y. Jung, G. W. Lee, C. E. Lee, H. S. Kang, J. Lee, K. B. Kim, D. Y. Ryu, S. Yu and C. Park, *Adv. Funct. Mater.*, 2021, **31**, 2008548.

11 S. Li, Y. Zeng, W. Hou, W. Wan, J. Zhang, Y. Wang, X. Du and Z. Gu, *Mater. Horiz.*, 2020, **7**, 2944–2950.

12 Y. Wang, Y. Yu, J. Guo, Z. Zhang, X. Zhang and Y. Zhao, *Adv. Funct. Mater.*, 2020, **30**, 2000151.

13 Y. Yang, Y. Chen, Z. Hou, F. Li, M. Xu, Y. Liu, D. Tian, L. Zhang, J. Xu and J. Zhu, *ACS Nano*, 2020, **14**, 16057–16064.

14 S. U. Kim, S. H. Lee, I. H. Lee, B. Y. Lee, J. H. Na and S. D. Lee, *Opt. Express*, 2018, **26**, 13561.

15 A. C. Arsenault, D. P. Puzzoo, I. Manners and G. A. Ozin, *Nat. Photonics*, 2007, **1**, 468–472.

16 H. Fudouzi and Y. N. Xia, *Langmuir*, 2003, **19**, 9653–9660.

17 J. Hou, M. Li and Y. Song, *Angew. Chem. Int. Ed.*, 2018, **57**, 2544–2553.

18 Y. Cui, Y. Ke, C. Liu, Z. Chen, N. Wang, L. Zhang, Y. Zhou, S. Wang, Y. Gao and Y. Long, *Joule*, 2018, **2**, 1707–1746.

19 C. Xiong, J. Zhao, L. Wang, H. Geng, H. Xu and Y. Li, *Mater. Horiz.*, 2017, **4**, 862–868.

20 Z. Li, J. Jin, F. Yang, N. Song and Y. Yin, *Nat. Commun.*, 2020, **11**, 1–11.

21 Y. Bao, Y. Yu, H. Xu, C. Guo, J. Li, S. Sun, Z. Zhou, C. Qiu and X. Wang, *Light Sci. Appl.*, 2019, **8**, 95.

22 B. M. Boyle, T. A. French, R. M. Pearson, B. G. McCarthy and G. M. Miyake, *ACS Nano*, 2017, **11**, 3052–3058.

23 J. Hou, M. Li and Y. Song, *Nano Today*, 2018, **22**, 132–144.

24 J. Chen, J. Feng, Z. Li, P. Xu, X. Wang, W. Yin, M. Wang, X. Ge and Y. Yin, *Nano Lett.*, 2019, **19**, 400–407.

25 A. G. Dumanlia and T. Savin, *Chem. Soc. Rev.*, 2016, **45**, 6698–6724.

26 Y. Li, Q. Fan, X. Wang, G. Liu, L. Chai, L. Zhou, J. Shao and Y. Yin, *Adv. Funct. Mater.*, 2021, 2010746.

27 E. Yablonovitch, *Phys. Rev. Lett.*, 1987, **58**, 2059–2062.

28 Z. Li and Y. Yin, *Adv. Mater.*, 2019, 1807061.

29 J. Ge and Y. Yin, *Angew. Chem. Int. Ed.,*2011, **50**, 1492–1522.

30 H. Ma, Y. Tan, J. Cao, S. C. Lian, K. Chen, W. Luo and J. Guan, *J. Mater. Chem. C*, 2018, **6**, 4531–4540.

31 L. He, M. Wang, J. Ge and Y. Yin, *Acc. Chem. Res.*, 2012, **45**, 1431–1440.

32 F. Yang, F. Mou, Y. Jiang, M. Luo, L. Xu, H. Ma and J. Guan, *ACS Nano*, 2018, **12**, 6668–6676.

33 L. Bai, Z. Xie, W. Wang, C. Yuan, Y. Zhao, Z. Mu, Q. Zhong and Z. Gu, *ACS Nano*, 2014, **8**, 11094–11100.

34 X. Jia, T. Zhang, J. Wang, K. Wang, H. Tan, Y. Hu, L. Zhang and J. Zhu, *Langmuir*, 2018, **34**, 3987–3992.

35 M. Wang and Y. Yin, *J. Am. Chem. Soc.*, 2016, **138**, 6315–6323.

36 Z. Li, M. Wang, X. Zhang, D. Wang, W. Xu and Y. Yin, *Nano Lett.*, 2019, **19**, 6673–6680.

37 Z. Li, F. Yang and Y. Yin, *Adv. Funct. Mater.*, 2019, 1903467.

38 W. Luo, H. Ma, F. Mou, M. Zhu, J. Yan and J. Guan, *Adv. Mater.*, 2014, **26**, 1058–1064.

39 H. Wang, Q. Chen, Y. Yu, K. Cheng and Y. Sun, *J. Phys. Chem. C*, 2011, **115**, 11427–11434.

40 J. Ge, L. He, J. Goebl and Y. Yin, *J. Am. Chem. Soc.*, 2009, **131**, 3484–3486.

41 C. Li, X. Zhou, K. Wang, K. Li, M. Li and Y. Song, *Compos. Commun.*, 2019, **12**, 47–53.

42 Y. Zhao, L. Shang, Y. Cheng and Z. Gu, *Acc. Chem. Res.*, 2014, **47**, 3632–3642.

43 J. Ge, H. Lee, L. He, J. Kim, Z. Lu, H. Kim, J. Goebl, S. Kwon and Y. Yin, *J. Am. Chem. Soc.*, 2009, **131**, 15687–15694.

44 W. Luo, J. Yan, Y. Tan, H. Ma and J. Guan, *Nanoscale*, 2017, **9**, 9548–9555.

45 S. Shang, Z. Liu, Q. Zhang, H. Wang and Y. Li, *J. Mater. Chem. A*, 2015, **3**, 11093–11097.

46 H. Wang, Q. Chen, Y. Sun and M. He, *J. Phys. Chem. C*, 2010, **114**, 19660–19666.

47 Y. Hu, L. He and Y. Yin, *Angew. Chem. Int. Ed.*, 2011, **50**, 3747–3750.

48 H. Ma, K. Tang, W. Luo, L. Ma, Q. Cui, W. Li and J. Guan, *Nanoscale*, 2017, **9**, 3105–3113.

49 W. Luo, Q. Cui, K. Fang, K. Chen, H. Ma and J. Guan, *Nano Lett.*, 2020, **20**, 803–811.

50 L. Kong, Y. Feng, W. Luo, F. Mou, K. Ying, Y. Pu, M. You, K. Fang, H. Ma and J. Guan, *Adv. Funct. Mater.*, 2020, 2005243.

51 J. M. Weissman, H. B. Sunkara, A. S. Tse and S. A. Asher, *Science*, 1996, **274**, 959–963.

52 F. Mou, C. Chen, Q. Zhong, Y. Yin, H. Ma and J. Guan, *ACS Appl. Mater. Interfaces*, 2014, **6**, 9897–9903.

53 H. Ma, M. Zhu, W. Luo, W. Li, K. Fang, F. Mou and J. Guan, *J. Mater. Chem. C*, 2015, **3**, 2848–2855.

54 K. Matsubara, M. Watanabe and Y. Takeoka, *Angew. Chem. Int. Ed.*, 2007, **46**, 1688–1692.

55 T. T. Perkins, D. E. Smith and S. Chu, *Science*, 1997, **276**, 2016–2021.

56 D. E. Smith and S. Chu, *Science*, 1998, **281**, 1335–1340.

57 D. Lisjak and A. Mertelj, *Prog. Mater. Sci.*, 2018, **95**, 286–328.

58 J. Wei, F. Song and J. Dobnikar, *Langmuir*, 2016, **32**, 9321–9328.

59 X. Xue and E. P. Furlania, *Phys. Chem. Chem. Phys.*, 2014, **16**, 13306–13317.